



Structural, linear/nonlinear optical and electrical studies on PVP/CMC blend filled with hydrogen titanate nanotubes and TMAI

A. M. El-naggar¹ · Zein K. Heiba² · A. M. Kamal³ · Mohamed Bakr Mohamed²

Received: 7 June 2023 / Accepted: 20 September 2023 / Published online: 7 October 2023

© The Author(s), under exclusive licence to Springer Science+Business Media, LLC, part of Springer Nature 2023

Abstract

In this study, the optical and electrical characteristics of a PVP/CMC blend have been improved by doping with hydrogen titanate nanotubes (HTNT) and tetramethylammonium iodide (TMAI) for adaptable eco-friendly applications. Undoped and doped PVP/CMC/HTNT/x wt% TMAI blends were formed using casting procedure, $x=0.0, 0.05, 0.1, 0.15, 0.2$. HRTEM micrographs of HTNT manifested a tubular structure. XRD measurements manifested a clear modification in the structure of the PVP/CMC blend owing to HTNT/TMAI doping. Diffuse reflectance and transmittance measurements revealed a big enhancement in absorption, in the range 250–400 nm, with a clear reduction in transmittance of PVP/CMC blend upon loading HTNT/TMAI, especially for $x=0.1$. The direct and indirect bandgaps (4.86, 4.36 eV) for PVP/CMC were reduced attaining minimum values (2.87, 3.46) and 2.99 eV for $x=0.15$ and 0.1 wt% TMAI, respectively. Also, the refractive index of the blend increased especially for the Vis/IR region (~ 1.35) getting a maximum value (2.85) for $x=0.1$. The influence of HTNT/TMAI doping on the different optical parameters: absorption coefficient, optical density, dielectric constant, optical conductivity, optical surface resistance, thermal emissivity and nonlinear optical parameters has been explored. The fluorescence intensities and CIE chromaticity coordinates of doped blends are affected by the excitation wavelength and the kind of fillers. From dielectric measurements, blends doped with 0.15 and 0.2 wt% TMAI have a higher capacitive nature than the undoped blend. Except for the blend containing 0.1 wt% TMAI, which possesses the highest energy density, all doped blends were found to have the lowest energy density compared to the undoped blend. The AC conductivity reached its highest value as the amount of TMAI doping became 0.15 wt%.

Keywords PVP · CMC · HTNT · TMAI ratios · Structure · Optical · Electrical

✉ Mohamed Bakr Mohamed
mbm1977@yahoo.com

¹ Research Chair of Exploitation of Renewable Energy Applications in Saudi Arabia, Physics & Astronomy Department, College of Science, King Saud University, P.O. Box 2455, 11451 Riyadh, Saudi Arabia

² Physics Department, Faculty of Science, Ain Shams University, Cairo, Egypt

³ Physics & Astronomy Department, College of Science, King Saud University, P.O. Box 2455, 11451 Riyadh, Saudi Arabia

1 Introduction

The synergistic or complementary behaviors of inorganic/organic nanocomposites are not found in their single-component counterparts, resulting in materials with superior functionality and applicability (El-naggar 2023a, b, c, f).

Carboxymethyl cellulose (CMC) is a semi-crystalline biodegradable material with excellent film forming ability. It is inexpensive, safe for the environment, and biodegradable (Abutalib and Rajeh 2020). Polyvinyl pyrrolidone (PVP) is a vinyl polymer with basically polar side groups in the ring and a planar molecular structure. PVP is semicrystalline and has a relatively high glass transition temperature for a substance in the pyrrolidone family (Alghunaim 2019).

The high chemical stability and activity, low cost, and nontoxicity of titanium dioxide (TiO_2) have made it a talented material for many uses. TiO_2 has an optical band gap of 3.0 and 3.2 eV for the rutile and anatase phases, respectively. It is well established that when exposed to UV light, TiO_2 nanoparticles generate electron–hole pairs. TiO_2 photocatalyst has been used effectively in the removal of organic pollutants from water and air as well as the destruction of bacteria (Camposeco et al. 2018). Furthermore, the unique properties and potential applications of titania and titanate nanotubes (TNT) in many fields such as proton conductivity, photocatalytic features, lithium transport and photovoltaic behavior have led to extensive study of these materials (Fernández-Werner et al. 2017). TNTs have garnered a lot of interest due to their superior adsorption capacity, lower toxicity, and lower environmental impact compared to TiO_2 particles (An et al. 2013). Moreover, hydrogen titanate nanotubes (HTNT) have a direct band gap of 3.3 eV and can be used in dye sensitized solar cell applications (Pignanelli et al. 2018).

The properties of polymers or blended polymers can be modified by doping them with the appropriate substance. For example, high-performance Z-scheme photocatalysts for CO_2 conversion was attained using in-situ synthesized porphyrin polymer/ TiO_2 composites (Zhang et al. 2021). Doing polyethylene oxide (PEO)/carboxymethyl cellulose (CMC) blend with nano ZnO and TiO_2 lead to use such nanocomposites in a diversity of energy-related devices, such as flexible capacitors, and energy storage systems (Ragab 2023). Mixing nano- TiO_2 with polymethyl methacrylate (PMMA) improved the host polymer's morphology and optical features, as evidenced by the blend's high structure stability, large dielectric constant, reduced optical bandgap, and higher nonlinear optical characteristics. This makes the TiO_2 /PMMA nanocomposite polymers promising materials for use in a variety of optoelectronic devices (AlAbdulaal and Yahia 2021). PEG/ TiO_2 composite outperforms PVA/ TiO_2 in photocatalytic and antibacterial activities (Tekin et al. 2020). Jayanthi et al. studied the influence of nano TiO_2 on the transport, and thermal features of PEMA-NaI solid polymer electrolytes and they found that the formed composite is suitable for energy storage devices (Jayanthi et al. 2022). Che et al. fabricated ultraviolet photodetectors based on TiO_2 nanorod arrays/PEDOT-type conducting polymers (Che et al. 2021). Liu et al. designed ultraviolet sensor-based TiO_2 nanorods/PProDOT-Pz conducting polymer using different bias voltages (Liu et al. 2022). Batteries, microelectronic devices, and energy storage devices are just a few of the many possible uses for the versatile CMC/PEO-LiCl/ TiO_2 nanocomposites samples (Al-Balawi 2023). Heiba et al. doped polyvinyl chloride (PVC) polymer with TiO_2 and tetrabutylammonium iodide (TBAI) and they found that PVC/ TiO_2 polymer doped with 25 wt% TBAI has maximum shielding for UVA and UVB types. AC conductivity increased by increasing TBAI amounts in PVA/ TiO_2 composite (Heiba et al. 2023). Mostafa et al. found that increasing HTNT content in PANI/

hydrogen titanate nanotube (HTNT) composite improved the thermal stability of polyaniline (Mostafa et al. 2016).

Furthermore, conductivity and dye-sensitized solar cell efficiency were improved by the addition of potassium iodide to a tetrapropylammonium iodide-polyvinyl alcohol-based gel polymer electrolyte (Aziz et al. 2021). Adding tetramethylammonium iodide (TMAI) to DPP-thieno [3, 2-b] thiophene-conjugated polymer increases hole mobility by a factor of 24 compared to thin films without the ionic additive under the same conditions (Luo et al. 2016).

The purpose of the current work is to upgrade the functional properties of the polymer blend PVP/CMC via loading with hydrogen titanate nanotubes (HTNT) and tetramethylammonium iodide (TMAI) to obtain novel nanocomposite for optoelectronic applications. So, the impact of HTNT and TMAI doping on the structural, electrical and optical properties of the PVP/CMC blend has been studied in detail. The developments in optical features and modifications in the electrical properties in the current study pave the way for the use of the flexible PVP/CMC/HTNT/x wt% TMAI blends in a wide diversity of optoelectronic applications.

2 Methods and materials

Hydrogen titanate nanotube (HTNT) was synthesized by the hydrothermal method using TiO_2 (anatase, 99%, Sigma-Aldrich, USA) as precursor as described before in the literature (Mostafa et al. 2016). The PVP/CMC (50/50%) and PVP/CMC/HTNT/x wt% TMAI blends were produced applying casting technique analogous to the preparation in Ref. (Luterotti 2010), using 0.5 g polyvinyl pyrrolidone (PVP, MW=40,000 g/mol, Alfa Aesar, USA), 0.5 g carboxymethyl cellulose, sodium salt (CMC, Sigma-Aldrich, USA), 5 wt% HTNT, x wt% TMAI (tetramethylammonium iodide, 99%, Sigma-Aldrich, USA, $x=0.05, 0.1, 0.15, 0.2$) and deionized water. The produced blend films have a thickness of 160–210 μm (digital micrometer with accuracy $\pm 10 \mu\text{m}$).

X-ray diffraction data was gathered with the help of a PANalytical diffractometer (X'Pert MPD, Philips, copper source). The HTNT sample's nanoscale characteristics were examined with a high-resolution transmission electron microscope (JEOL JEM-2100, 200 keV). UV diffused reflectance (R), transmittance (T) and absorbance (A) data for the blends were obtained using diffused reflectance spectrophotometer (JASCO-V-670, with attached integrating sphere assembly) system. A luminescence spectrophotometer (FP-8200 JASCO) was used to acquire the fluorescence (FL) spectra.

By applying an ac voltage of 2 V and measuring the resulting change in capacitance (C) and dissipation factor ($\tan \delta$), one can calculate the dielectric constant as a function of frequency ($f=100 \text{ Hz}-1 \text{ MHz}$) at RT. The subsequent relations (Rodríguez-Carvajal 1993) were employed to compute the complex electric modulus ($M^*=M'+iM''$), ac conductivity (σ_{ac}), and dielectric constant (ϵ' , ϵ'') of all blends:

$$\epsilon' = \frac{dC}{\epsilon_0 A} \quad (1)$$

$$\sigma_{ac} = 2\pi f \epsilon_0 \epsilon' \tan \delta \quad (2)$$

$$\tan\delta = \varepsilon''/\varepsilon' \quad (3)$$

$$M' = \frac{\varepsilon'}{\varepsilon'^2 + \varepsilon''^2} \quad (4)$$

$$M'' = \frac{\varepsilon''}{\varepsilon'^2 + \varepsilon''^2} \quad (5)$$

where ε_0 and A are the permittivity of free space and area of the disk, respectively.

3 Results and discussion

3.1 Structural investigation

The x-ray diffractogram obtained for the prepared HTNT is depicted in Fig. 1a. The pattern represents a typical layered titanate (Morgado et al. 2006), especially the peak at $2\theta = 10.5^\circ$ which is attributed to the interlayer distance. All other peaks matched well with the standard pattern of a protonic layered titanate, $\text{H}_2\text{Ti}_3\text{O}_7 \cdot 3\text{H}_2\text{O}$ with orthorhombic unit cell space group P mmm (Camposeco and Hinojosa-Reyes 2022; Bavykin et al. 2006), indicating a complete conversion of anatase (TiO_2) to hydrogen titanate. HRTEM micrographs of the sample, Fig. 1b, manifested a tubular structure with a nearly uniform diameter of an average value 7.5 nm, and tube lengths averaging from 50 to 95 nm. The corresponding SAED pattern given in Fig. 1c disclosed diffraction rings with interplanar spacings that matched with the reported ones (Morgado et al. 2006; Camposeco and Hinojosa-Reyes 2022).

The x-ray diffractograms measured for the polymer blend PVP/CMC pure and loaded with 5% HTNT/ x wt% TMAI are given in Fig. 1d. Diffractogram of undoped PVP/CMC polymer blend manifested a high diffused scattering background with two humps around 15° and 20° with a very small diffraction peak at 41° , indicating the amorphous nature of the blend. Upon loading with HTNT or TMAI, the diffraction patterns retain the same features with a change in the intensity of the two humps indicating interaction between the functional groups of blend components and HTNT and/or TMAI molecules. For TMAI content of $x = 0.15$ and 0.2 wt%, two small diffraction peaks appeared at 15.3° and 22.1° correspond to TMAI (Aziz et al. 2022). The degree of crystallinity (X_{cry} %) was calculated using the Hermans–Weidinger approach and listed in Table 1 (Gusev 1978).

3.2 Optical features

The UV-diffused absorbance (A), transmittance (T) and reflectance (R) data over the UV–visible regions for undoped and doped PVP/C/C/HTNT/ x wt% TMAI blended polymers with HTNT and TMAI are represented in Fig. 2a–c. For wavelengths shorter than 240 nm, it is evident that the doped blends have lower absorbance than the pure blend. Above this range the situation is reversed where the absorbance achieved its supreme value beyond this range up to 350 nm as the blend doped with 0.1 wt% HTNT after that sample with 0.2 wt% HTNT exhibited the slightly highest absorbance. All blends with HTNT exhibited an absorption band at ~ 217 nm while doped blends with TMAI have extra absorbance band at 289 nm. These bands associated with the $n \rightarrow \pi^*$ electronic transition (oxazine rings in the

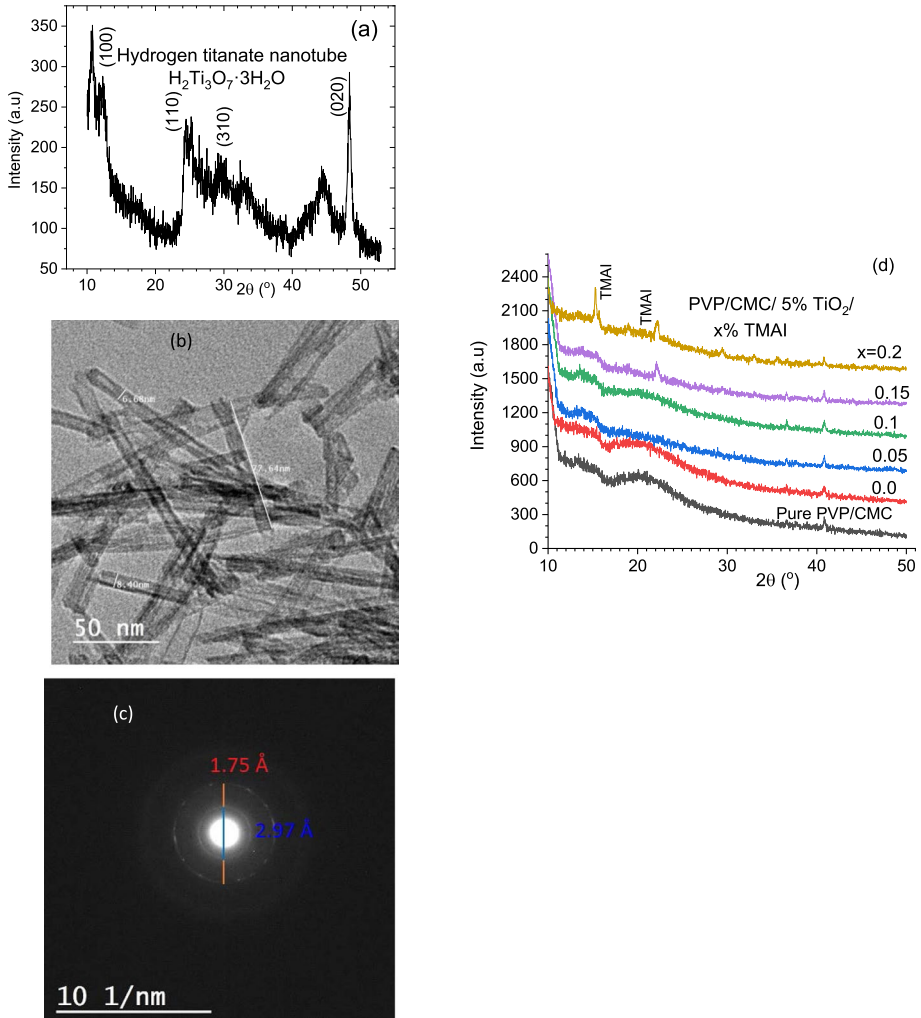


Fig. 1 **a** XRD data of HTNT, **b** HRTEM pattern for HTNT, **c** SAED for HTNT and **d** XRD diffraction data for undoped and doped PVP/CMC with HTNT and TMAI

Table 1 Direct and indirect optical band gap energies and crystallinity for undoped and doped PVP/CMC with HTNT/TMAI

	Direct E_g (eV)	Indirect E_g (eV)	X_{cry} %
PVP/CMC	4.86	4.36	8
PVP/CMC/HTNT/x wt% TMAI			
x = 0	3.55, 4.73	3.14	8
x = 0.05	3.53, 4.67	3.12	6
x = 0.1	3.42, 4.62	2.99	7
x = 0.15	2.87, 3.46	3.00	10
x = 0.2	3.22, 3.45	3.06	12

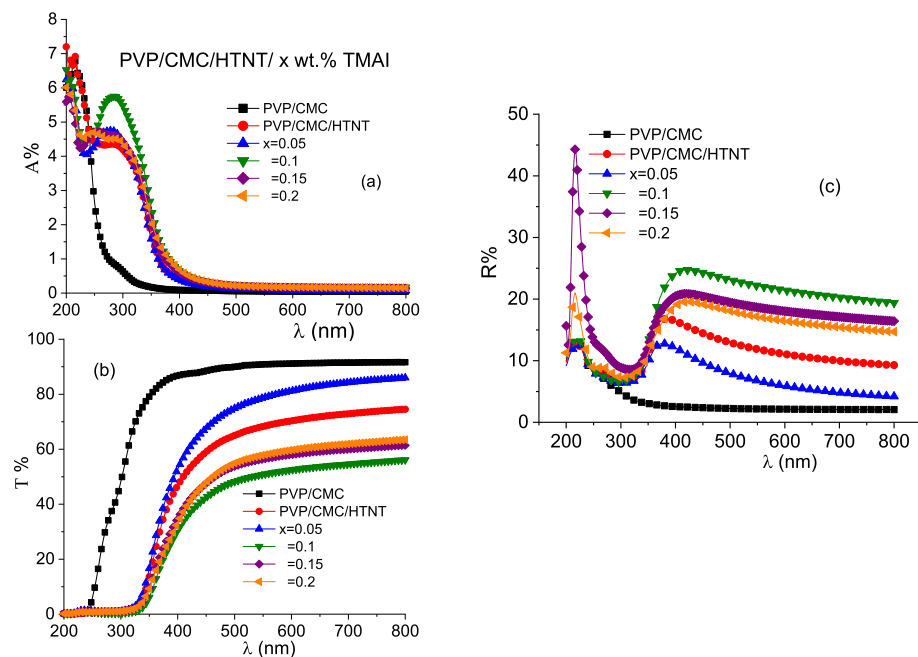


Fig. 2 **a** Absorbance, **b** transmittance and **c** reflectance spectra for undoped and doped PVP/CMC with HTNT and TMAI

blended system) and the main benzenoid $\pi \rightarrow \pi^*$ kind transitions, respectively (Luo et al. 2016). In addition, redshifts were noticed in the absorbance edges of the doped blends relative to the undoped blend. This finding suggested that the optical bandgap of the resulting mixture had reduced. Similar reductions were observed as the amounts of ZnO/TiO₂ or TiO₂ were increased in PEO/CMC blend (Ragab 2023) or PMMA/FTO polymeric nanocomposite films (AlAbdulaal and Yahia 2021). The graph demonstrated also the doped PVP/CMC blended polymers with HTNT and/or TMAI have good absorbance of UV light at 315–380 nm (UVA) and 280–315 nm (UVB) as compared with the undoped blend. The UVB absorbance was enhanced as the blend doped with HTNT and 0.1 wt% TMAI. A similar result was gotten as PVP/CMC was loaded with natural melanin (El-naggar et al. 2023d). Additionally, the transmittance of blend doped with HTNT reduced and it reduced further irregularly as the amounts of TMAI rose and it reached its lowest value as the blend was doped with 0.1 wt% TMAI. Doped blends also have a higher reflectance spectrum than their undoped counterparts. Maximum reflectance was achieved for wavelengths up to 350 nm when the blend was loaded with 0.15 wt% TMAI; for wavelengths beyond this range, the highest R values were achieved by the blend loaded with 0.1 wt% TMAI. Changes in the packing density of the blend upon doping with different amounts of fillers (Kafashan et al. 2016) may account for the observed variation in reflectance across the various blends. As a result of HTNT and/or TMAI doping, blends' absorbance is enhanced, and their optical transmittance is tailored, opening new possibilities for use in optical devices (Vigneshwaran et al. 2012). Also, the PVP/CMC/HTNT/0.15 wt% TMAI blend is recommended for use in a wide variety of applications, including warning signs, lifesaving marks, and advertising, due to its high reflectance in the visible range (El-naggar et al. 2023d). Changing T

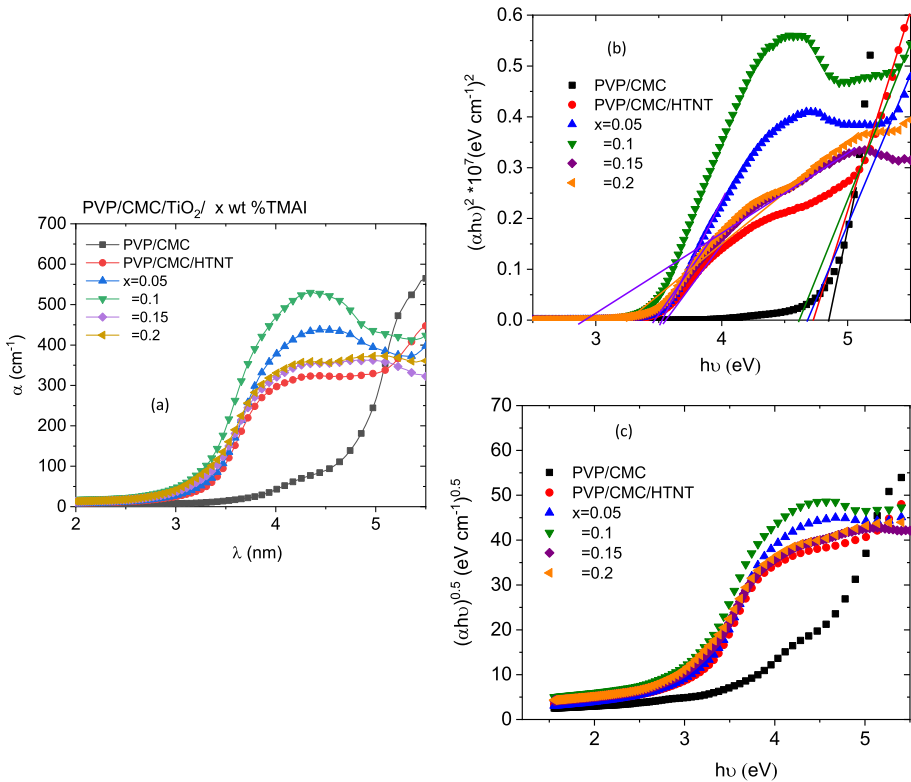


Fig. 3 a Relation between $\ln\alpha$ and $h\nu$, Tauc relation for **b** direct and **c** indirect optical band gaps for undoped and doped PVP/CMC with HTNT and TMAI

and R will affect the optical band gap, refractive index, optical sheet resistance and other optical parameters.

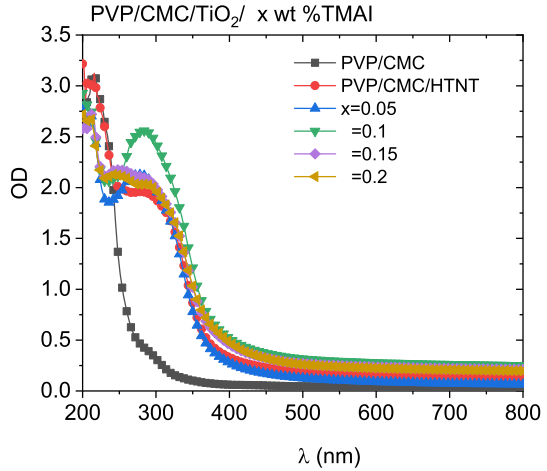
The optical energy bandgap (E_g) was calculated for all blends using the following Tauc’s expression (El-naggar et al. 2022a):

$$\alpha h\nu = B(h\nu - E_g)^q \tag{6}$$

where h , ν , B , α ($=2.303A/d$), and t are Planck’s constant, incident light frequency, a constant, absorption coefficient, and thickness of the blend, respectively. $q=0.5$ or 2 for direct and indirect optical band transitions, respectively.

The absorption coefficient (α), $(\alpha h\nu)^{1/2}$, $(\alpha h\nu)^2$, and $\ln(\alpha)$ versus the photon energy ($h\nu$) for PVP/CMC/HTNT/ x wt% TMAI blends are revealed in Fig. 3a–c, respectively. The absorption coefficient passes two steps: (1) α slightly raised with raising $h\nu$ up to 2.5 and 3 eV in the case of undoped and doped blends, respectively, and (2) for photon energy above 3 eV, α is raised exponentially with growing $h\nu$. At 2.5 eV, the calculated α is 5.66, 12.54, 12.13, 22.23, 16.67, 17.9 cm^{-1} for undoped and doped PVP/CMC with HTNT, $x=0.05$, 0.1, 0.15 and 0.2 wt% TMAI, respectively. Above these ranges, α shows a dramatic rise in its value. For example, at 4.5 eV, undoped and doped PVP/CMC with HTNT, $x=0.05$, 0.1, 0.15 and 0.2 wt% TMAI blends, respectively, have of $\alpha=89.99$, 322.91, 437.78, 524.21, 355.03 and 356.97 cm^{-1} , respectively.

Fig. 4 The optical density (OD) as function of wavelength for undoped and doped PVP/CMC with HTNT and TMAI



The $(\alpha h\nu)^2$ and $(\alpha h\nu)^{0.5}$ curves vs. $h\nu$ are plotted in Fig. 3b, c, respectively, to determine the direct and indirect (E_{dirg} and E_{indg}) optical bandgaps of undoped and doped PVP/CMC blends. The E_g values of films are found at the $h\nu = 0$ intercepts of the extrapolated linear parts of the plotted curves. E_{dirg} and E_{indg} values are shown for each blend in Table 1. The E_{dirg} and E_{indg} values for PVP/CMC blend are 4.86 and 4.36 eV, respectively. These values were reduced to their minimum values, (2.87, 3.46) eV and 2.99 eV for E_{dirg} and E_{indg} , respectively, as the PVP/CMC doped with HTNT and $x = 0.15$ and 0.1 wt% TMAI, respectively. The formation of defects within the blend as a result of the doping with the fillers is responsible for this reduction. These defects formed localized states inside the blended polymer (host matrix) that facilitated the transfer of electrons from HOMO (highest-occupied molecular orbital) and LUMO (lowest unoccupied molecular orbital) and hereafter decreased the optical band gap of the blend. Similar results were observed as the amounts of tetrabutylammonium iodide (TBAI) or LiCl/TiO₂ nanoparticles increased in PVC/TiO₂ polymer or CMC/PEO blended polymer (Al-Balawi 2023; Heiba et al. 2023). The appearance of two band gaps in doped blends may assign to the blend and the filler materials.

Optical density (OD) vs. wavelength for each blend is plotted in Fig. 4. The OD is computed as follows (Abd-Elnaiem et al. 2023; Tezel and Karipe 2019):

$$OD = -\log_{10}(T) \quad (7)$$

The value of OD displayed two distinct stages: (1) In the wavelength ranges 200–350 and 200–450 nm in the case of undoped and doped blends, respectively, values of OD are dramatically reduced with raising the incident wavelength. (2) Above 350 and 450 nm in the case of undoped and doped blends, respectively, OD values attained steady values for the remaining part of the investigated wavelength. Comparing A and OD curves, both A and OD have alike performance with wavelength.

The refractive index (n), extinction coefficient (k), optical surface resistance (R_s) and thermal emissivity (ϵ_{th}) of the various blends were computed by Abd-Elnaiem et al. (2023); El-naggar et al. 2022b; Tezel et al. 2019):

$$n = \frac{1+R}{1-R} + \sqrt{\frac{4R}{(1-R)^2} - k^2} \quad (8)$$

$$k = \frac{\lambda\alpha}{4\pi} \quad (9)$$

$$R_s = -\frac{4\pi}{c} \cdot \frac{1}{n \cdot \ln(T)} \quad (10)$$

$$\varepsilon_{th} = 1 - \frac{1}{[1 + (2\varepsilon_o c R_s)]^2} \quad (11)$$

where c and ε_o are the speed of light and permittivity of free space, respectively.

Figure 5 represents the variation of n , k , R_s and ε_{th} as functions of the frequency. It can be seen in Fig. 5a that the n performance is like the reflectance spectra shown in Fig. 2b. Up to about $\lambda=400$ nm, the n value of the PVP/CMC blend decreased as the λ increased, but after that, it remained roughly constant as the wavelength increased in the visible range. Where, the n value of the PVP/CMC blend reduces as the wavelength is raised up to 400 nm, it has a quasi-steady behaviour as λ is raised further in the visible range. As the blend was doped with HTNT and/or TMAI, the n value was enhanced as compared with the undoped PVP/CMC. Also, its value is affected by the measured λ range. It accomplished its highest value in the UV region as the blend was doped with $x=0.15$ wt% TMAI. In the visible range, n achieved its highest value as the blend was doped with $x=0.1$ wt% TMAI. Figure 5b represents the variation of n values with changing amounts of TMAI doping. The graph shows that adding HTNT to the PVP/CMC blend raised the value of n , while adding TMAI in varying amounts led to irregular rise in n value. At 500 nm, the n value attained its highest value as it was doped with 0.1 wt% TMAI. This improvement may provide evidence for the higher reflectance of the blends as a result of the greater number of reflecting centres and the higher density of the loaded blends compared to the pure ones (El-naggar et al. 2022c, d). Previous work, such as that involving TBAI doped PVC/TiO₂ (Heiba et al. 2023), yielded similar results.

As can be seen in Fig. 5c, k behaved in a manner analogous to the absorbance performance shown in Fig. 2a. It reduced abruptly as the λ increased in the UV range. The quasi-steady state for k value is achieved as λ increased in the visible range. Additionally, up to 250 nm, the doped blends' k values are lower than those of the undoped blends. This situation is reversed beyond this wavelength range. This finding is credited with the changes in the absorbance performance of the different blends. As revealed from Fig. 5d, e both R_s and ε_{th} displayed similar tendencies, where they raised as λ increased. Also, both values are reduced irregularly as the blend doped with HTNT and/or different amounts from TMAI.

In order to reveal their use in optoelectronic and energy applications, the dielectric properties of all blends were investigated. The real (ε_r) and imaginary (ε_i) dielectric constant parts, optical conductivity (σ_{opt}), surface energy loss function (SELF) and volume energy loss function (VELF) of the different blends can be gotten from Kumar et al. (2018); Kariper and Özpozan 2014):

$$\varepsilon_r = n^2 - k^2 \quad (12)$$

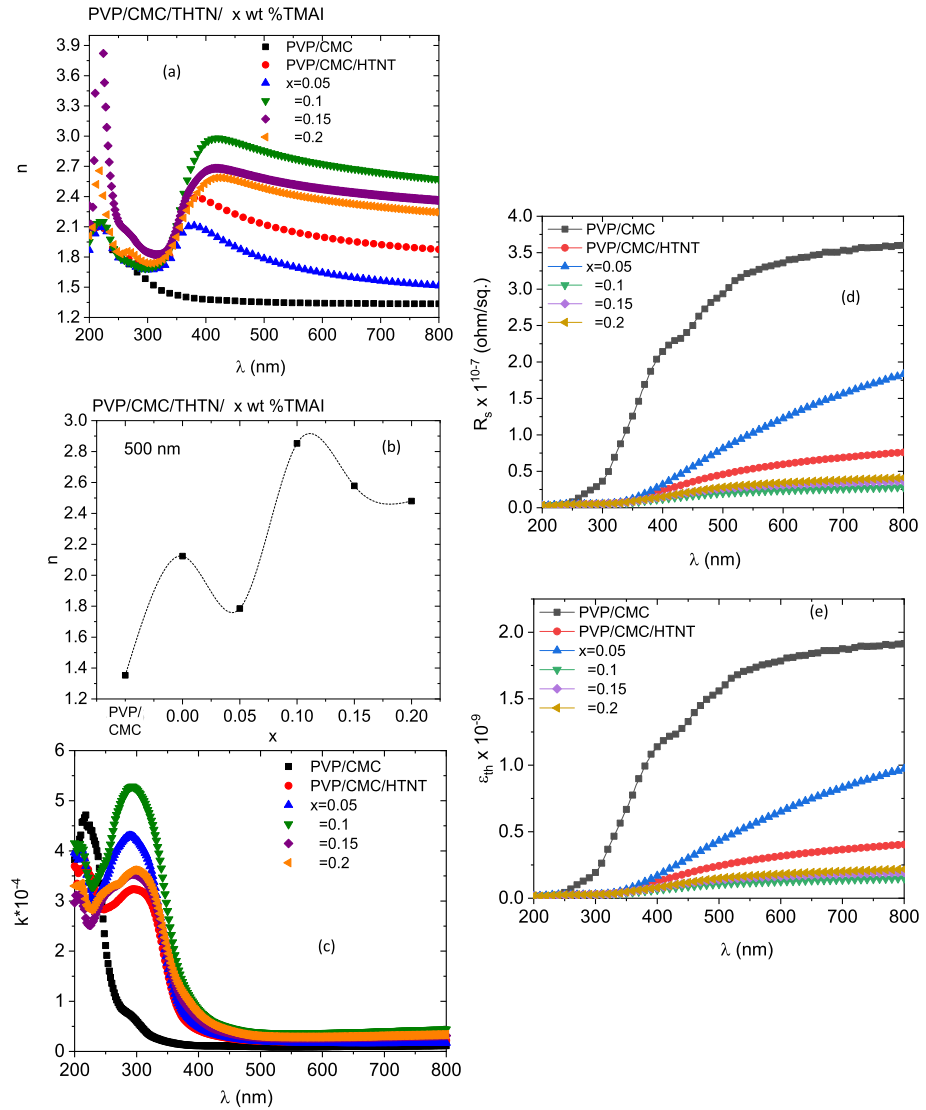


Fig. 5 **a** Refractive index, **b** extinction coefficient as function of the wavelength, **c** variation of refractive index as function of doping, **d** optical surface resistance and **e** thermal emissivity for undoped and doped PVP/CMC with HTNT and TMAI

$$\epsilon_i = 2nk \tag{13}$$

$$\sigma_{opt} = \frac{anC}{4\pi} \tag{14}$$

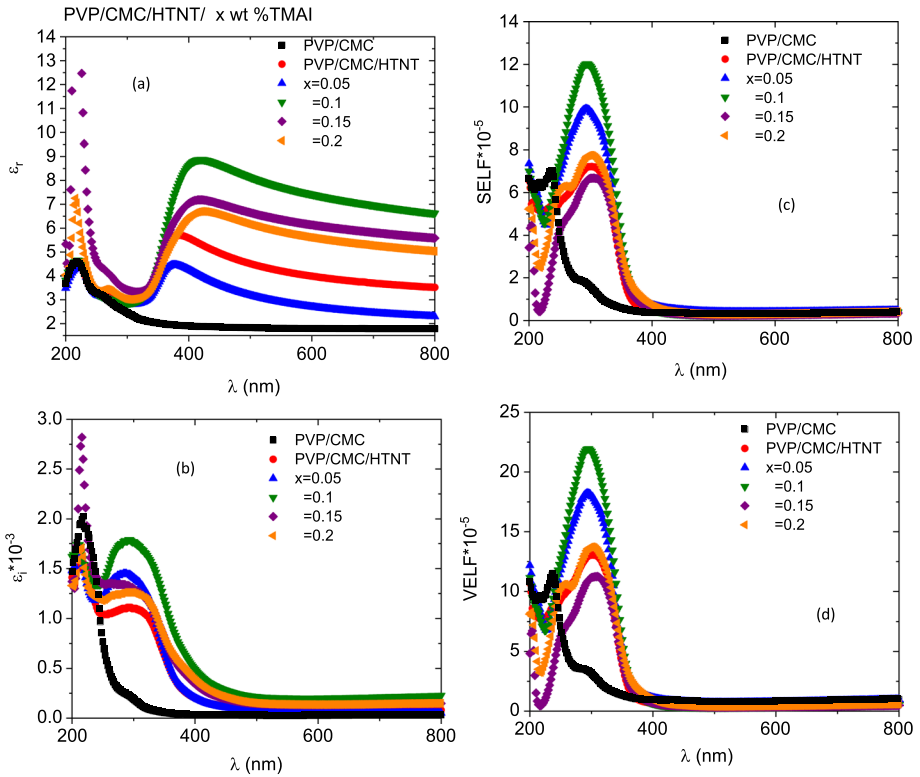


Fig. 6 The altering of **a** real and **b** imaginary dielectric constant, **c** SELF and **d** VELF with the wavelength for undoped and doped PVP/CMC with HTNT and TMAI

$$SELF = \frac{\epsilon_i}{(\epsilon_r + 1)^2 + \epsilon_i^2} \tag{15}$$

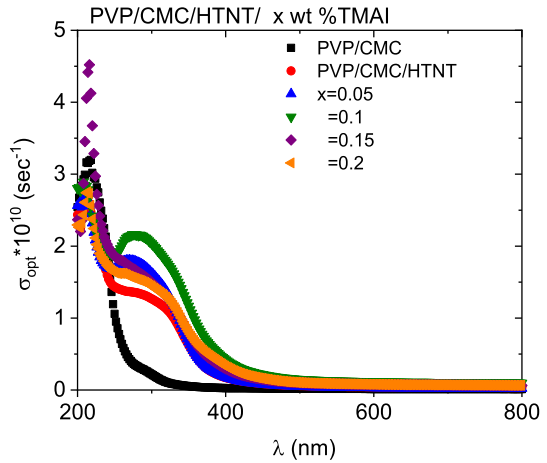
$$VELF = \frac{\epsilon_i}{\epsilon_r^2 + \epsilon_i^2} \tag{16}$$

where C is velocity of the light.

The wavelength dependence of the dielectric property’s two components (real ϵ_r and imaginary ϵ_i) is shown in Figs. 6a and b. A similar behaviour between the real permittivity and the refractive index n is observed. Doped blended polymers with nanofillers also have larger ϵ_r values than undoped blend across whole λ range. A similar behaviour is noticed in the performance of the imaginary part ϵ_i of the dielectric constant in the wavelength beyond 250 nm, while in the wavelength 200–250, the situation is reversed. Because of their improved real dielectric part ϵ_r , doped polymers are more suitable for use as energy storage devices (Zhu et al. 2021). Whereas the ϵ_i performance reveals the capability to lose more energy as a result of doping with nanofillers in the visible range.

There are two ways to quantify the interaction of incident electromagnetic radiation with electrons in a sample when it transports through its surface or penetrates its mass: the surface energy loss function (SELF) and the volume energy loss function (VELF). Figure 6c,

Fig. 7 Optical conductivity for undoped and doped PVP/CMC with HTNT and TMAI



d depicts the wavelength-dependent changes in VELF and SELF. The performances of the SELF and VELF data are comparable. The calculated value of SELF is lower than VELF value for the entire wavelength range which indicates that very little energy is lost from the surface during propagation through the bulk material. Besides, both SELF and VELF spectra were raised in doped blends relative to the undoped blend at wavelengths larger than 250 nm.

Using the absorption coefficient and refractive index n , we were able to determine the optical conductivity (σ_{opt}) of both undoped and doped PVP/CMC blends (Fig. 7). Doped blends have a smaller σ_{opt} in the 200–250 nm range compared to undoped blends. Beyond this range, σ_{opt} rose as the PVP/CMC doped with HTNT and/or TMAI. σ_{opt} values are thought to have changed as a result of the modification in the rate of photon absorption, which affected the number of electrons that were formed (Ismail et al. 2022).

Both undoped and doped blends’ nonlinear optical (NLO) properties in the UV–visible spectral range are investigated.

The linear optical susceptibility ($\chi^{(1)}$), nonlinear third order optical susceptibility ($\chi^{(3)}$), and nonlinear refractive index (n_2) of the blends were computed using the next formula (El-naggar et al. 2022e):

$$\chi^{(1)} = \frac{1}{4\pi} (n^2 - 1) \tag{17}$$

$$\chi^{(3)} = 1.7 * 10^{-10} (\chi^{(1)})^4 = 1.7 * 10^{-10} \left(\frac{n^2 - 1}{4\pi} \right)^4 \tag{18}$$

$$n_2 = \frac{12\pi}{n} \chi^{(3)} \tag{19}$$

Figure 8 depicts the frequency-dependent changes in $\chi^{(1)}$, $\chi^{(3)}$ and n_2 for all blends. Non-linear optical parameters ($\chi^{(1)}$, $\chi^{(3)}$ and n_2) of doped blends are shown to be enhanced across the entire wavelength range compared to those of an undoped blend. NLO parameters in the visible range reach their highest values in a doped blend with $x=0.1$ wt% TMAI. These findings may be due to its larger refractive index n in this region. Improvement of the

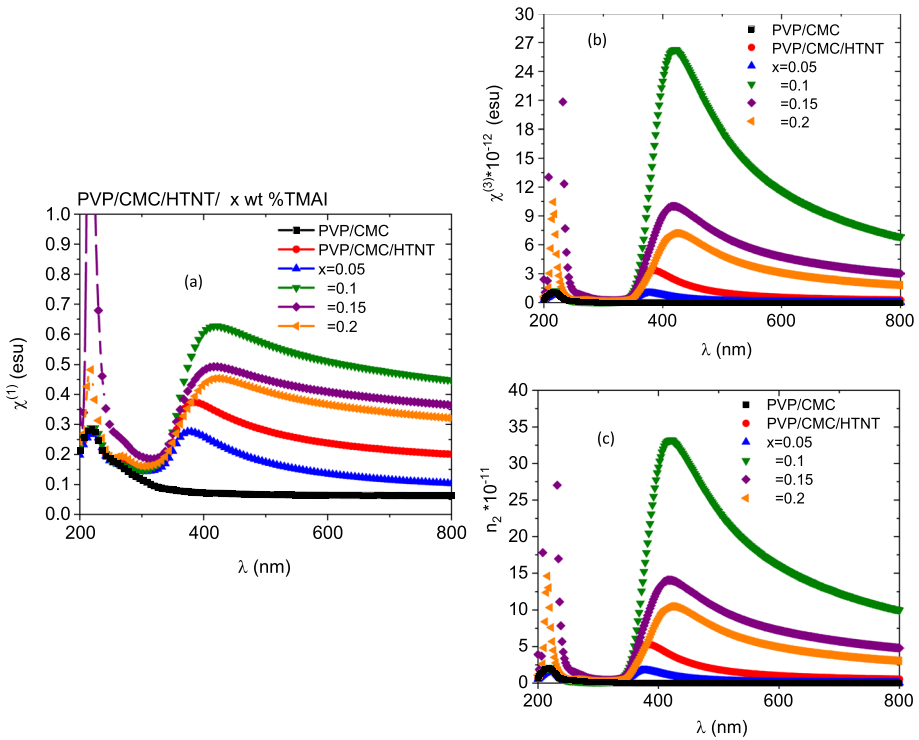


Fig. 8 a-c Wavelength dependent of the nonlinear optical parameters for undoped and doped PVP/CMC with HTNT and TMAI

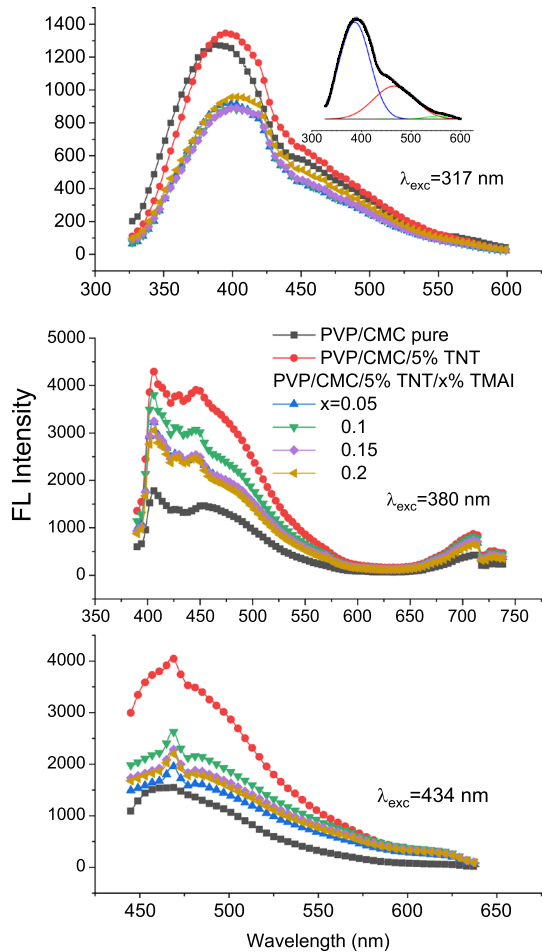
nonlinear optical characteristics of doped PVP/CMC with HTNT and/or TMAI nominates them for updated applications in high-speed communications and fast optical switching.

3.3 Fluorescence analysis

Under excitation $\lambda_{\text{exc}} = 317$ nm, the FL spectrum of undoped PVP/CMC blend a broad-spectrum peak at 398 nm with a saddle to the right, Fig. 9a. The spectrum is red shifted and the FL intensity is increased under excitation $\lambda_{\text{exc}} = 380$ and 434 nm, Fig. 9b, c. Decomposition of the spectrum applying Gaussian fitting exposed two main bands at 386 nm (violet) and 465 nm (blue) and a very weak peak at 557 nm (green). The main bands are attributed to the $n \leftarrow n\pi^*$ transition in n -electrons of the C=O moieties in PVP (Behera and Ram 2015), and in the $-\text{OH}$ groups of CMC.

Under $\lambda_{\text{exc}} = 270$ nm, PVP disclosed a strong broad spectrum with multiple maxima at 370, 410 and 436 nm resulting from the electronic transitions of carbonyl group C=O group (Joseph and Mathew 2021). Under $\lambda_{\text{exc}} = 325$ nm, PVP revealed a broad spectrum with a peak maximum was observed at 394 nm (Thi et al. 2012). The pure CMC film features no optical properties (Li et al. 2018), however, CMC showed fluorescent nature depending on the solvent used in order of increasing polarity; methylene chloride, DMSO, or methanol (Wang et al. 2010). Due to the presence of the $-\text{OH}$ (hydroxyl) and (COO^-) (carboxylate) groups, CMC polymer can form a gel, blend with other polymers

Fig. 9 FL data for undoped and doped PVP/CMC with HTNT and TMAI under different excitation wavelengths



soluble in water, and react effectively with ionic dopants (Morsi et al. 2019a). The PVP/CMC components are miscible and interact together via hydrogen bond formation between the $-OH$ of cellulose of CMC and the carbonyl group ($C=O$) of PVP (Morsi et al. 2019b). Doping PVC/CMC blend with HTNT enhanced the FL intensity a little for $\lambda_{exc} = 317$ nm and highly for $\lambda_{exc} = 380$ and 434 nm, Fig. 9b, c. Interactions occur between HTNT and the functional groups of blend components (Abdelghany et al. 2015), carbonyl group ($C=O$) of PVP and the carboxylate group (COO^-) of CMC. These interactions cause the chains of polymer composite to wind around the filler particles which introduce distortions for the helical conformation of PVP/CMC blend and hence stretch the helical conformation to make zigzag arrangements (Koduru et al. 2017; Morsi et al. 2018). Upon loading TMAI, interactions between the functional groups of blend components and TMAI molecules initiate delocalization in PVP/CMC. TMAI may connect with one or more PVP/CMC polymer repeating units forming trap sites prohibiting the electron-hole recombination process. Figure 10 displays CIE chromaticity diagrams for both undoped and doped PVP/CMC blends, while Table 2 provides the corresponding CIE chromaticity coordinates (x , y). Both undoped and doped PVP/CMC emitted a blue light when excited at 317 and 380 nm.

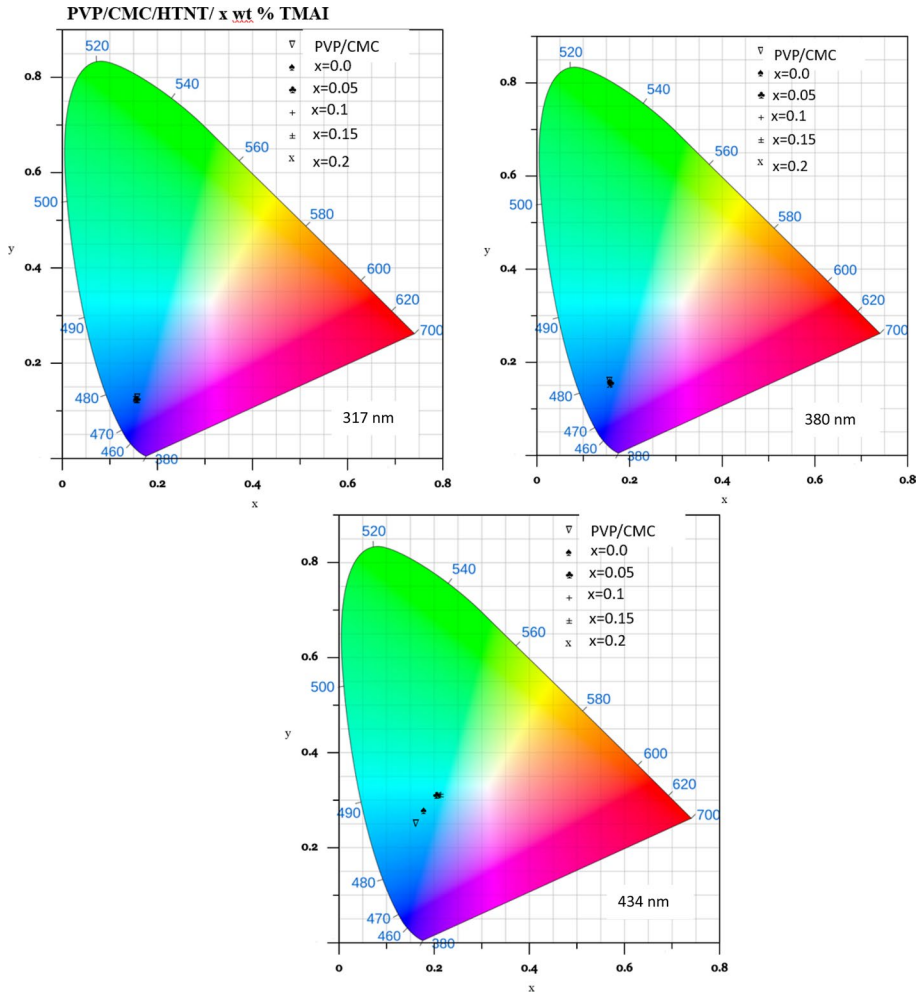


Fig. 10 CIE diagram for undoped and doped PVP/CMC with HTNT and TMAI under different excitation wavelengths

Table 2 Chromaticity coordinates (x, y) for the FL spectra denoted in Fig. 9

	317 nm	380 nm	434 nm
PVP/CMC	(0.1566, 0.1282)	(0.1558, 0.1597)	(0.1613, 0.2508)
PVP/CMC/HTNT/x wt% TMAI			
x = 0	(0.1554, 0.1243)	(0.1567, 0.1584)	(0.1784, 0.2776)
x = 0.05	(0.1558, 0.1239)	(0.1578, 0.1547)	(0.2042, 0.3097)
x = 0.1	(0.1557, 0.1239)	(0.1575, 0.1534)	(0.2025, 0.3106)
x = 0.15	(0.1559, 0.1226)	(0.1584, 0.1577)	(0.2129, 0.3133)
x = 0.2	(0.1554, 0.1258)	(0.1578, 0.1522)	(0.2087, 0.3110)

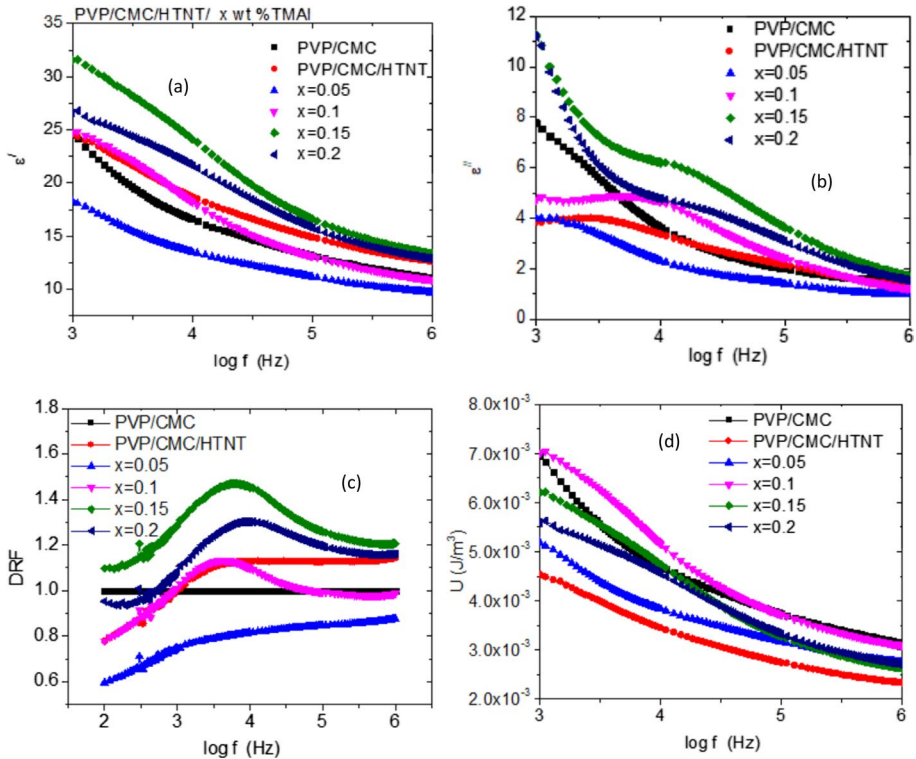


Fig. 11 The **a** real, **b** imaginary parts of the dielectric constant, **c** DRF and **d** energy density for undoped and doped PVP/CMC with HTNT and TMAI

Under excitation at 434 nm, the color index of all blends was found to increase. Where the color turns towards the green region as the blend is doped with HTNT/TMAI. Enhancement of FL intensity nominates the nano composite PVP/CMC/5% HTNT as a promising material for light-emitting diode and solar cell.

3.4 Dielectric characteristics

Measurements of dielectric properties yield important data for the most efficient design of materials used in dielectric applications. The ability of a material to polarize and store electrical charges when utilized as a capacitor is measured via the real part of the dielectric constant (ϵ'), while the imaginary part is the dielectric loss (ϵ'') creating throughout the development and alignment of dipoles (Taha and Azab 2019). Figure 11a, b represents the variations of ϵ' and ϵ'' as functions of logarithm frequency for all samples. As revealed from the graphs the values of ϵ' and ϵ'' rose sharply at low frequencies since dipoles in the film favor aligning themselves in the direction of the applied field. At higher frequencies, the charge cannot follow the applied field, reducing the dielectric permittivity (Ramesh and Liew 2013). Figure 11a demonstrates that by adding HTNT to PVP/CMC blend, ϵ' increased at lower frequency range and increased slightly at the higher frequency range. By adding 0.05 wt% HTNT to the

above composite, the ϵ' decreased. The highest ϵ' value, indicating the highest concentration of dissociated ions, is achieved in a system composed of PVP/CMC/HTNT/0.15 wt% HTNT. A similar result was detected as PEMA/NaI doped with 4 wt% TiO₂ (Jayanthi et al. 2022). Also, the values of ϵ' and ϵ'' improved with rising LiCl/TiO₂ amounts, achievement its greatest value at PEO@CMC-15 wt% of LiCl/TiO₂ (Al-Balawi 2023). In contrast, as PEO/CMC blend doped with ZnO/TiO₂ both ϵ' and ϵ'' decreased (Ragab 2023). Furthermore, the dipolar ordering of polar PVP/CMC was impacted by the electrostatic interactions of the fillers, leading to different values of dielectric permittivity for the doped blend (El-naggar et al. 2023e). Increases in the value of ϵ' indicated a greater capability of the host matrix to store energy (Al-Muntaser et al. 2023). The ϵ'' value dropped when HTNT was added to the mixture, rose irregularly as TMAI was added, and peaked when the TMAI concentration was 0.15 wt%. Differences in the charge carrying capacity of the blend after doping with different fillers cause this variation in the value of ϵ'' (Morgado et al. 2006).

The ability of the polymer to achieve normalized polarization is said to be expressed by the dielectric reinforcing function (DRF), according to the next relation (Taha and Alzara 2021):

$$DRF = \frac{\epsilon'(\text{nanocomposite})}{\epsilon'(\text{pureblend})} \quad (20)$$

Figure 11c shows the calculated DRF function of all blends. In terms of polarization response, the sample with 0.2 wt% MATI is clearly superior to the others.

It is possible to calculate the energy density (U) of a material, which is defined as the amount of energy it can store in a given volume using the next formula (Taha and Alzara 2021):

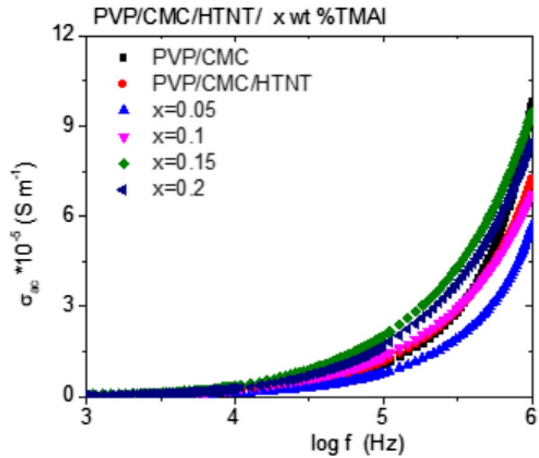
$$U = \frac{1}{2} \epsilon_0 \epsilon' E^2 \quad (21)$$

where ϵ' , ϵ_0 and E are the dielectric permittivity, permittivity of free space (8.85×10^{-12} F/m) and the electric field, respectively.

Figure 11d, represents the variation of U as function of frequency for all blends. The graph shows that all blends have lower energy densities than the pure blend, except for the blend doped with 0.1 wt% TMAI, which has the highest energy densities.

The AC conductivity (σ_{ac}) of all blends is shown to be frequency (f)-dependent in Fig. 12. The graph clearly shows that ac grew larger at higher frequencies. Because polymers have non-equilibrium trap charges, the σ_{ac} in the low-frequency region varies slightly with f . Reduced conductivity is a result of an increase in charge accumulation at the electrode/electrolyte interface (Al-Muntaser et al. 2020). Not only that, but after a certain frequency value, it grew exponentially. Frequency-dependent conductivity in polymer composites is caused by hopping transport between localized states (Abdullah et al. 2016). Additionally, as the blend doped with HTNT, σ_{ac} changed slightly then decreased as it was doped with 0.05 wt% TMAI. By increasing the amount of TMAI in the PVP/HTNT/x wt% TMAI, the σ_{ac} increased irregularly and it reached its highest value as the amount of TMAI became 0.15 wt%. The changes in the electrical conductivity might be attributed to the modification in the space-charge polarization (Chen et al. 2017). In addition, the gap between localized states within the blend was modified by changes in the concentration of TMAI, which in turn modified the potential barriers separating them and thus altered the flow of the charges (Al-hakimi et al. 2022).

Fig. 12 The ac conductivity for undoped and doped PVP/CMC with HTNT and TMAI

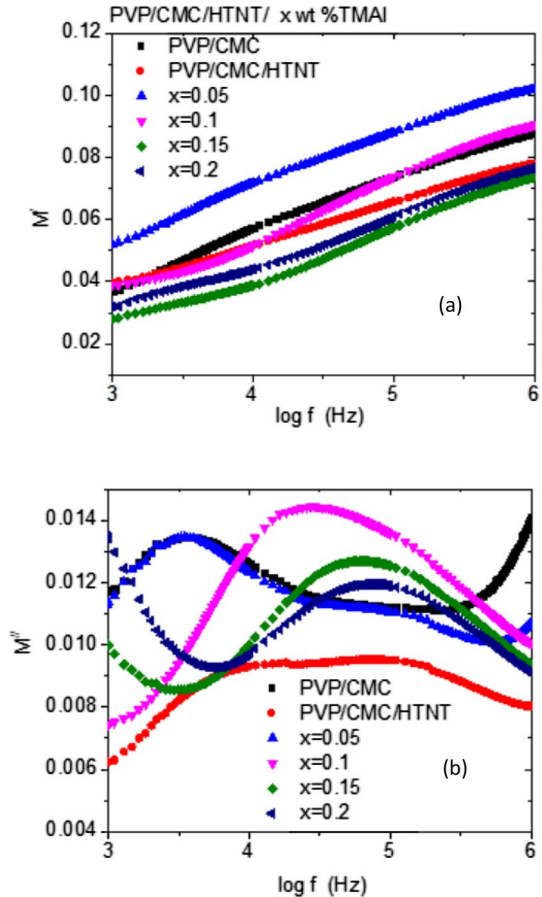


Using the complex electric modulus, the phenomenon of conductivity relaxation has been investigated. The electrode influence is omitted by this formalization. There is an advantage to knowing the difference between bulk effects and electrode polarization phenomena (Ragab 2023). Figure 13a, b depicts the pure and doped PVP/CMC blends' real (M') and imaginary (M'') electric moduli as a function of f . Frequency-dependent M' values for all blends showed step-like plots, and relaxation peaks can be seen in the M'' spectra. Maxwell–Wagner–Sillars (MWS) dynamics, linked to structural heterogeneity, may account for this peak (Sengwa et al. 2019). The values of M' have low values in the lower frequency range because of the unimportant effect of electrode polarization, demonstrating that the electrode impact has a slight polarization (Sengwa et al. 2019). At lower frequencies, the value of M' was reduced as PVP/CMC/HTNT were loaded with 0.15 and 0.2 wt% TMAI, respectively. This indicated that these two sample blends have a higher capacitive nature than the undoped blend (Elashmawi et al. 2022). The M' values decreased in all doped blends except the blend with 0.05 wt% TMAI, where M' increased. Besides, the M'' spectra reflects the effect of both HTNT and TMAI, adding to the blend in the dynamics of the relaxation mechanism and the mobility of the charge carriers. The intensity of this peak diminished as the blend was doped with HTNT and/or different amounts of TMAI, except for the blend loaded with 0.1 wt% TMAI, where it increased. Also, the position of this peak is altered relative to the undoped blend according to the dopant amounts. The shift of the peak towards the lower/higher frequency range with changed HTNT and/or TMAI amounts is associated with the modification in conductivity (Pagot et al. 2018). These alternations indicated the interaction of fillers with the host PVP/CMC matrix. Non-Debye and ionic conductivity can be inferred from the presence of a single relaxation peak and a wide relaxation spread (Al-Balawi 2023). Also, all doped blends have a lower relaxation time except those with 0.05 wt% HTNT.

4 Conclusion

XRD and HRTEM investigation of the HTNT nanofiller revealed a tubular structure with orthorhombic unit cell and uniform tube diameter. XRD of PVP/CMC/HTNT/TMAI composite disclosed an amorphous structure with some diffraction peaks characteristic of

Fig. 13 The **a** real and **b** imaginary parts of electric modulus for undoped and doped PVP/CMC with HTNT and TMAI



TMAI enhanced absorbance of UVA and UVB types. The direct/indirect optical bandgaps of the blend were reduced as it doped with HTNT and reduced further as it doped with TMAI in addition. (n) increased with adding HTNT or TMAI, but irregularly with TMAI content. Also, R_s and ϵ_{th} were reduced while the optical dielectric and optical conductivity increased, all nonmonotonically with TMAI content; obviously, interaction between the functional groups of the PVP/CMC blend and TMAI molecules is dependent on the TMAI content. The FL intensity was enhanced for PVP/CMC/HTNT, while upon loading TMAI, it decreased nonmonotonically with its content, but retaining values higher than pure PVP/CMC blend. Under excitation at 434 nm, the color turns towards the green region as the blend is doped with HTNT/TMAI. The blend with 0.2 wt% TMAI has the highest dielectric reinforcing function. All composites have lower energy densities than the pure blend, except for that with 0.1 wt% TMAI. σ_{ac} reached its highest value for the composite with 0.15 wt% TMAI. All doped blends have a lower relaxation time except those with 0.05 wt% HTNT. Based on these optical and electrical results, PVP/CMC doped with HTNT/TMAI are candidates for use in flexible and environmentally friendly applications.

Acknowledgements The authors extend their appreciation to the Deputyship for Research & Innovation, Ministry of Education in Saudi Arabia for funding this research. (IFKSURC-1-1019)

Authors' contribution All authors have contributed, discussed the results and approved the final manuscript.

Funding This work is supported by Deputyship for Research & Innovation, Ministry of Education in Saudi Arabia.

Data availability The authors confirm that the data supporting the findings of this study are available within the article.

Declarations

Conflict of interest The authors declare that they have no conflict of interest.

Ethical approval We agreed on all terms and conditions for ethics approval.

References

- Abdelghany, A., Mekhail, M.S., Abdelrazek, E., Aboud, M.: Combined DFT/FTIR structural studies of monodispersed PVP/Gold and silver nano particles. *J. Alloy. Compd.* **646**, 326 (2015)
- Abd-Elnaiem, A.M., Rashad, M., Hanafy, T.A., Shaalan, N.M.: Improvement of optical properties of functionalized polyvinyl alcohol-zinc oxide hybrid nanocomposites for wide UV optoelectronic applications. *J. Inorgan. Organomet. Polym. Mater.* (2023). <https://doi.org/10.1007/s10904-023-02616-w>
- Abdullah, O.G., Salman, Y.A.K., Saleem, S.A.: Electrical conductivity and dielectric characteristics of in situ prepared PVA/HgS nanocomposite films. *J. Mater. Sci. Mater. Electron.* **27**, 3591 (2016)
- Abutalib, M.M., Rajeh, A.: Structural, thermal, optical and conductivity studies of Co/ZnO nanoparticles doped CMC polymer for solid state battery applications. *Polym. Test.* **91**, 106803 (2020)
- AlAbdulaal, T.H., Yahia, I.S.: Optical linearity and nonlinearity, structural morphology of TiO₂-doped PMMA/FTO polymeric nanocomposite films: laser power attenuation. *Optik Int. J. Light Electron Optic.* **227**, 166036 (2021)
- Al-Balawi, S.A.: nSynthesis of LiCl/TiO₂ nanoparticles and their influence study on the structural, optical, and conductivity properties of CMC/PEO polymer composite as an application in optoelectronic devices. *Opt. Mater.* **138**, 113613 (2023)
- Alghunaim, N.S.: Effect of CuO nanofiller on the spectroscopic properties, dielectric permittivity and dielectric modulus of CMC/PVP nanocomposites. *J. Market. Res.* **8**(4), 3596 (2019)
- Al-hakimi, A.N., Asnag, G.M., Alminderej, F., Alhagri, I.A., Al-Hazmy, S.M., Abdallah, E.M.: Enhanced structural, optical, electrical properties and antibacterial activity of selenium nanoparticles loaded PVA/CMCblend for electrochemical batteries and food packaging applications. *Polym. Test.* **116**, 107794 (2022)
- Al-Muntaser, A.A., Abdelghany, A.M., Abdelrazek, E.M., Elshahawy, A.G.: Enhancement of optical and electrical properties of PVC/PMMA blend films doped with Li₄Ti₅O₁₂ nanoparticles. *J. Mater. Res. Technol.* **9**, 789 (2020)
- Al-Muntaser, A.A., Pashameah, R.A., Alzahrani, E., AlSubhi, S.A., Hameed, S.T., Morsi, M.A.: Graphene nanoplatelets/TiO₂ hybrid nanofiller boosted PVA/CMC blend based high performance nanocomposites for flexible energy storage applications. *J. Polym. Environ.* **31**, 2534 (2023)
- An, Y., Li, Z., Shen, J.: The visible light absorption property of Cu-doped hydrogen titanate nano tube thin films: an experimental and theoretical study. *Phys. B* **429**, 127 (2013)
- Aziz, M.F., Azam, M.A., Buraidah, M.H., Arof, A.K.: Effect of the potassium iodide in tetrapropyl ammonium iodide-polyvinyl alcohol-based gel polymer electrolyte for dye-sensitized solar cells. *Optik* **247**, 167978 (2021)
- Aziz, M.F., Azam, M.A., Yusuf, S.N.F., Buraidah, M.H., Arof, A.K.: Influence of potassium iodide in polyvinyl alcohol-based gel polymer electrolyte for efficiency enhancement of dye-sensitized solar cells. *J. Polym. Res.* **29**, 455 (2022)
- Bavykin, D.V., Friedrich, J.M., Walsh, F.C.: Protonated titanates and TiO₂ nanostructured materials: synthesis, properties, and applications. *Adv. Mater.* **18**, 2807 (2006)
- Behera, M., Ram, S.: Fullerenes. Nanotubes Carbon Nanostruct. **23**, 1064 (2015)

- Camposeco, R., Castillo, S., Rodríguez-González, V., Hinojosa-Reyes, M., Medina-Álvarez, M.I., Mejía-Centeno, I.: Promotional effect of Rh nanoparticles on WO₃/TiO₂ titanate nanotube photocatalysts for boosted hydrogen production. *J. Photochem. Photobiol. A Chem.* **353**, 114 (2018)
- Camposeco, R., Hinojosa-Reyes, M., Zanella, R.: Behavior of the energy levels of hydrogen titanate nanotubes decorated with Au, Ag, Mn, and Ni and their effect on the H₂ evolution. *Top. Catal.* **65**, 989 (2022)
- Che, Y., Zhang, H., Abdiryim, T., Jamal, R., Kadir, A., Helil, Z., Liu, H.: Ultraviolet photodetectors based on TiO₂ nanorod arrays/PEDOT-type conducting polymers. *Opt. Mater.* **122**, 111805 (2021)
- Chen, X., Tseng, J.K., Treufeld, I., Mackey, M., Schuele, D.E., Li, R., Zhu, L.: Enhanced dielectric properties due to space charge-induced interfacial polarization in multilayer polymer films. *J. Mater. Chem. C* **5**(39), 10417 (2017)
- Elashmawi, I.S., Al-Muntaser, A.A., Ismail, A.M., Structural, M.: optical, and dielectric modulus properties of PEO/PVA blendfilled with metakaolin. *Opt. Mater.* **126**, 112220 (2022)
- El-naggar, A.M., Heiba, Z.K., Kamal, A.M., Abd-Elkader, O.H., Lakshminarayana, G., Mohamed, M.B.: Structural, thermal, and linear/nonlinear optical performance of PVA/CMC polymer blend doped with ZnS/V prepared at different temperatures. *J. Polym. Res.* **29**(11), 1 (2022a)
- El-naggar, A.M., Heiba, Z.K., Kamal, A.M., Altowairqi, Y., Mohamed, M.B.: Impact of loading PVA/CMC/PVP blend with CdS_{0.9}M_{0.1} non-stoichiometrically doped by transition metals (M). *Optic. Mater.* **133**, 113085 (2022b)
- El-naggar, A.M., Heiba, Z.K., Mohamed, M.B., Kamal, A.M., Lakshminarayana, G., Shar, M.A.: Structural, linear and nonlinear optical properties of poly (vinyl alcohol) (PVA)/polyethylene glycol (PEG)/SnS₂: Y nanocomposite films. *Optik* **258**, 168941 (2022c)
- El-naggar, A.M., Heiba, Z.K., Kamal, A.M., Lakshminarayana, G., Abd-Elkader, O.H., Mohamed, M.B.: Preparation of PVA/CMC/PVP blended polymer loaded with ZnS_{1-x}Cu_x; investigation of structural and linear/nonlinear optical properties. *Opt. Mater.* **133**, 113066 (2022d)
- El-naggar, A.M., Heiba, Z.K., Kamal, A.M., Altowairqi, Y., Mohamed, M.B., Abd-Elkader, O.H., Alhazime, A.A.: Influence of nanocomposite (1-x) CdS/xCuS on optical characteristics of PVA/CMC/PEG blended polymer; effect of ratio (x). *Opt. Mater.* **133**, 112923 (2022e)
- El-naggar, A.M., Heiba, Z.K., Kamal, A.M., Abd-Elkader, O.H., Lakshminarayana, G., Mohamed, M.B.: Linear and nonlinear optical characteristics of PVA/CMC/PEG blended polymer loaded with ZnS formed at different temperatures. *J. Mater. Sci. Mater. Electron.* **34**(2), 114 (2023a)
- El-naggar, A.M., Heiba, Z.K., Kamal, A.M., Mohamed, M.B.: The role of cobalt amount in ZnCdS nanofiller on the optical, thermal, dielectric and structure properties of PVA/PVP/PEG blends. *Opt. Quant. Electron.* **55**(7), 609 (2023b)
- El-naggar, A.M., Alsaggaf, A., Heiba, Z.K., Kamal, A.M., Aldhafiri, A.M., Fatehmulla, A., Mohamed, M.B.: Exploring the structural, optical and electrical characteristics of PVA/PANi blends. *Opt. Mater.* **139**, 113771 (2023c)
- El-naggar, A.M., Heiba, Z.K., Kamal, A.M., Alzahrani, K.E., Abd-Elkader, O.H., Mohamed, M.B.: Impact of natural melanin doping on the structural, optical and dielectric characteristics of the PVP/CMC blend. *J. Taibah Univ. Sci.* **17**(1), 2190731 (2023d)
- El-naggar, A.M., Alsaggaf, A., Heiba, Z.K., Kamal, A.M., Aldhafiri, A.M., Mohamed, M.B.: *J. Taibah Univ. Sci.* **17**(1), 2207769 (2023e)
- El-Naggar, A.M., Heiba, Z.K., Kamal, A.M., Abd-Elkader, O.H., Mohamed, M.B.: Impact of ZnS/Mn on the structure, optical, and electric properties of PVC polymer. *Polymers* **15**(9), 2091 (2023f)
- Fernández-Werner, L., Pignanelli, F., Montenegro, B., Romero, M., Pardo, H., Faccio, R., Mombrú, Á.W.: Characterization of titanate nanotubes for energy applications. *J. Energy Storage* **12**, 66 (2017)
- Gusev, G.V.: Hermans-Weidinger X-ray diffraction technique for determining polymer crystallinity and the use of the Ruland ratio. *Polym. Sci. USSR* **20**(5), 1295 (1978)
- Heiba, Z.K., El-naggar, A.M., Kamal, A.M., Abd-Elkader, O.H., Mohamed, M.: Optical and dielectric properties of PVC/TiO₂/TBAI ionic liquid polymer electrolyte. *Optic. Mater.* **139**, 113764 (2023)
- Ismail, M.S., Elamin, A.A., Abdel-Wahab, F., Elbasha, Y.H., Mahasen, M.M.: Improving the refractive index by engineering PbS/PVA nano polymer composite for optoelectronic applications. *Opt. Mater.* **131**, 112639 (2022)
- Jayanthi, S., Shenbagavalli, S., Muthuvinayagam, M., Sundaresan, B.: Effect of nano TiO₂ on the transport, structural and thermal properties of PEMA-NaI solid polymer electrolytes for energy storage devices. *Mater. Sci. Eng. B* **285**, 115942 (2022)
- Joseph, A., Mathew, S.: Electronic properties of PVP-ionic liquid composite: spectroscopic and DFT-based thermochemical studies on the effect of anions. *Iran. Polym. J.* **30**, 505 (2021)
- Kafashan, H., Azizieh, M., Vatan, H.N.: Ultrasound-assisted electrodeposition of SnS: effect of ultrasound waves on the physical properties of nanostructured SnS thin films. *J. Alloy. Compd.* **686**, 962 (2016)

- Kariper, A., Özpozan, T.: Optical properties of cobalt xanthate films on different substrates. *Metall. Mater.* **21**(7), 736 (2014)
- Koduru, H., Marino, L., Scarpelli, F., Petrov, A., Marinov, Y., Hadjichristov, G., Iliev, M., Scaramuzza, N.: Structural and dielectric properties of NaIO₄-complexed PEO/PVP blended solid polymer electrolytes. *Curr. Appl. Phys.* **17**, 1518 (2017)
- Kumar, S., Supriya, S., Kar, M.: Enhancement of dielectric constant in polymer-ceramic nanocomposite for flexible electronics and energy storage applications. *Compos. Sci. Technol.* **157**, 48 (2018)
- Li, T., Li, B., Ji, Y., Wang, L.: Luminescent and UV-shielding ZnO quantum dots/carboxymethylcellulose sodium nanocomposite polymer films. *Polymers* **10**, 1112 (2018)
- Liu, H., Abdiryim, T., Jamal, R., Liu, X., Niyaz, M., Liu, L., Zhang, H., Zou, D., Li, J., Song, Y., Wei, J.: Ultraviolet sensor-based TiO₂ nanorods/PProDOT-Pz conducting polymer using different bias voltage. *Opt. Mater.* **129**, 112477 (2022)
- Luo, H., Yu, C., Liu, Z., Zhang, G., Geng, H., Yi, Y., Broch, K., Hu, Y., Sadhanala, A., Jiang, L., Qi, P., Cai, Z., Siringhaus, H., Zhang, D.: Remarkable enhancement of charge carrier mobility of conjugated polymer field-effect transistors upon incorporating an ionic additive. *Sci. Adv.* **2**, e1600076 (2016)
- Lutterotti, L.: Total pattern fitting for the combined size-strain-stress-texture determination in thin film diffraction. *Nucl. Inst. Methods Phys. Res. B* **268**, 334 (2010)
- Morgado, E., Jr., de Abreu, M.A., Pravia, O.R., Marinkovic, B.A., Jardim, P.M., Rizzo, F.C., Araújo, A.S.: A study on the structure and thermal stability of titanate nanotubes as a function of sodium content. *Solid State Sci.* **8**(8), 888–900 (2006)
- Morsi, M.A., Abdelaziz, M., Oraby, A.H., Mokhles, I.: Effect of lithium titanate nanoparticles on the structural, optical, thermal and electrical properties of polyethylene oxide/carboxymethyl cellulose blend. *J. Mater. Sci. Mater. Electron.* **29**, 15912 (2018)
- Morsi, M.A., Abdelaziz, M., Oraby, A.H., Mokhles, I.: Structural, optical, thermal, and dielectric properties of polyethylene oxide/carboxymethyl cellulose blend filled with barium titanate. *J. Phys. Chem. Solids* **125**, 103 (2019a)
- Morsi, M.A., Rajeh, A., Menazea, A.A.: Nanosecond laser-irradiation assisted the improvement of structural, optical and thermal properties of polyvinyl pyrrolidone/carboxymethyl cellulose blend filled with gold nanoparticles. *J. Mater. Sci. Mater. Electron.* **30**, 2693 (2019b)
- Mostafa, N.Y., Mohamed, M.B., Imam, N.G., Alhamyani, M., Heiba, Z.K.: Electrical and optical properties of hydrogen titanate nanotube/PANI hybrid nanocomposites. *Colloid Polym. Sci.* **294**, 215 (2016)
- Pagot, G., Bertasi, F., Vezzù, K., Nawn, G., Pace, G., Nale, A., Noto, V.D.: Correlation between properties and conductivity mechanism in poly(vinylalcohol)-based lithium solid electrolytes. *Solid State Ion.* **320**, 177 (2018)
- Pignanelli, F., Fernández-Werner, L., Romero, M., Mombrú, D., Tumelero, M.A., Pasa, A.A., Germán, E., Faccio, R., Mombrú, Á.W.: Hydrogen titanate nanotubes for dye sensitized solar cells applications: experimental and theoretical study. *Mater. Res. Bull.* **106**, 40 (2018)
- Ragab, H.M.: Optical, thermal and electrical characterization of PEO/CMC incorporated with ZnO/TiO₂ NPs for advanced flexible optoelectronic technologies. *Ceram. Int.* **49**, 12563 (2023)
- Ramesh, S., Liew, C.-W.J.M.: Dielectric and FTIR studies on blending of [xPMMA- (1-x) PVC] with LiTFSI. *J. Meas.* **46**(5), 1650–1656 (2013)
- Rodríguez-Carvajal, J.: Recent advances in magnetic structure determination by neutron powder diffraction. *Phys. B* **192**, 55 (1993)
- Sengwa, R.J., Choudhary, S., Dhatarwal, P.: Nonlinear optical and dielectric properties of TiO₂ nanoparticles incorporated PEO/PVP blend matrix based multi-functional polymer nanocomposites. *J. Mater. Sci. Mater. Electron.* **30**, 12275 (2019)
- Taha, T.A., Alzara, M.A.A.: Synthesis, thermal and dielectric performance of PVA-SrTiO₃ polymer nanocomposites. *J. Mol. Struct.* **1238**, 130401 (2021)
- Taha, T.A., Azab, A.A.: Thermal, optical, and dielectric investigations of PVC/La_{0.95}Bi_{0.05}FeO₃ Nanocomposites. *J. Mol. Struct.* **1178**, 39 (2019)
- Tekin, D., Birhan, D., Kiziltas, H.: Thermal, photocatalytic, and antibacterial properties of calcinated nano-TiO₂/polymer composites. *Mater. Chem. Phys.* **251**, 1230C67 (2020)
- Tezel, F.M., Karipe, İ.A.: A new process to synthesize CrSe thin films with nanosize by CBD method. *Mater. Res. Express* **6**, 036412 (2019)
- Tezel, N.S., Tezel, F.M., Kariper, İ.A.: Surface and electro-optical properties of amorphous Sb₂S₃ thin films. *Appl. Phys. A* **125**, 198 (2019)
- Thi, T.M., Tinh, L.V., Van, B.H., Ben, P.V., Trung, V.Q.: The effect of polyvinylpyrrolidone on the optical properties of the Ni-doped ZnS nanocrystalline thin films synthesized by chemical method. *J. Nanomater.* **2012**, 1–8 (2012)

- Vigneshwaran, M., Chandiramouli, R., Jeyaprakash, B.G., Balamurugan, D.: Physical properties of spray deposited Mg doped CdO thin films. *J. Appl. Sci.* **12**, 1754 (2012)
- Wang, C., Popescu, D.C., Wu, C., Zhu, J., Macklin, W., Wang, Y.: In situ fluorescence imaging of myelination. *J. Histochem. Cytochem.* **58**(7), 611 (2010)
- Zhang, Y., Zhang, G.-L., Wang, Y.-T., Ma, Z., Yang, T.-Y., Zhang, T., Zhang, Y.-H.: In-situ synthesized porphyrin polymer/TiO₂ composites as high-performance Z-scheme photocatalysts for CO₂ conversion. *J. Colloid Interface Sci.* **596**, 342 (2021)
- Zhu, D., Yang, Z., Zhao, J., Guo, H., Gao, L.: Ultrahigh energy density of polymer nanocomposites containing electrostatically self-assembled graphene oxide and hydrotalcite nanosheets. *Ceram. Int.* **47**, 33766 (2021)

Publisher's Note Springer Nature remains neutral with regard to jurisdictional claims in published maps and institutional affiliations.

Springer Nature or its licensor (e.g. a society or other partner) holds exclusive rights to this article under a publishing agreement with the author(s) or other rightsholder(s); author self-archiving of the accepted manuscript version of this article is solely governed by the terms of such publishing agreement and applicable law.